Intrinsic instability of Fe^{4+} in electrochemically oxidized ramsdellite and orthorhombic $Li_{1-x}H_xFeO_2$

L. Bordet-Le Guenne,[a] P. Deniard,*[a] A. Lecerf,[b] P. Biensan,[c] C. Siret,[c] L. Fournès[d] and R. Brec[a]

[a]Laboratoire de Chimie des Solides, IMN, 2 rue de la Houssinière, B.P. 32229, 44322, Nantes, cedex 3, France. E-mail: deniard@cnrs-imn.fr
[b]Laboratoire de Chimie des Solides, I.N.S.A., 20 avenue des Buttes de Coësmes, 35043, Rennes, cedex, France
[c]SAFT, Route de Nozay, 91460, Marcoussis, France
[d]ICMCB, 162 avenue du Dr. Schweitzer, 33608, Pessac, cedex, France

The cathodic materials r-$Li_{0.8}H_{0.2}FeO_2$ (ramsdellite-type) and o-$Li_{0.7}H_{0.3}FeO_2$ (orthorhombic form) were synthesized in an autoclave by reaction of iron oxohydroxides with lithium ethoxide in anhydrous ethanol. The compositions of the phases were determined both by means of elemental analyses and density measurements. The crystal structures of r-$Li_{0.8}H_{0.2}FeO_2$ and o-$Li_{0.7}H_{0.3}FeO_2$ were determined by the Rietveld method. The powders were made of homogeneously distributed submicronic needles. Electrochemical tests of the $Li_{1-x}H_xFeO_2$/Li systems were carried out along with X-ray diffraction and Mössbauer spectroscopy. The results from all the physical techniques employed taken together showed the instability of Fe^{4+} formed during the recharge of the $Li_{1-x}H_xFeO_2$ materials, forbidding cycling on the Fe^{4+}/Fe^{3+} electrochemical couple.

1 Introduction

Owing to its low cost and its non-toxicity, the $LiFeO_2$ oxide appears as an ideal cathodic material for lithium batteries. A dozen-odd $LiFeO_2$ phases have been reported to date in the literature. Several high temperature or hydrothermal-type syntheses have led to the preparation of several compact structure materials, for instance the α, β, β′, β″, γ and spinel phases.[1–9] Three other phases: l-$LiFeO_2$ (layered, isotypic of $LiCoO_2$), r-$LiFeO_2$ (ramsdellite type) and o-$LiFeO_2$ (orthorhombic form) have been recently studied.[10–20] Although written with a stoichiometric formula, these materials were reported as lithium deficient, with the probable occurrence of protons in place of lithium and no precise composition being given.

Up to now, the only two forms of $LiFeO_2$ found to be 'rechargeable' are the ramsdellite and the orthorhombic phases. However, the two materials present a poor reversibility the origin of which is not understood to date, with a very low discharge voltage (mean potential *ca.* 2.2 V).[16–18]

Because of these unexplained results and owing to the lack of analytical and structural information, the study of the iron analogues of r-MnO_2 and o-$LiMnO_2$ (fairly good electrochemical compounds themselves) was initiated. By coupling the analytical, electrochemical and structural data, a procedure not fully carried out yet, a more accurate picture of the properties and functioning of the ramsdellite and orthorhombic lithium iron oxides was expected. The results of such studies are reported here.
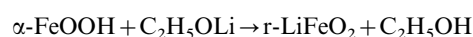
2 Experimental

2.1 Syntheses

The r-$Li_{0.80}H_{0.20}FeO_2$ and o-$Li_{0.70}H_{0.30}FeO_2$ phases (see elemental analyses below) have been obtained by reaction of a suspension of α-FeOOH and γ-FeOOH (*ca.* 4 g) in *ca.* 25 ml of anhydrous ethanol in a 300 ml autoclave with a slightly overstoichiometric amount of lithium ethoxide (Table 1). The mixtures were heated, under constant stirring, at 170 and 140 °C for 15 h, respectively. α-FeOOH and γ-FeOOH were prepared following the method of Brauer,[21] while C_2H_5OLi

Table 1 Elemental analyses for r-$Li_{1-x}H_xFeO_2$ and o-$Li_{1-x}H_xFeO_2$. The Li_2CO_3 quantities have been calculated assuming that all the carbon content was attributable to this salt
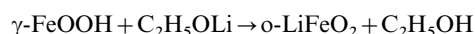
	Ramsdellite sample	Orthorhombic sample
Initial Li/Fe ratio	1.03	1.03
Li (wt%)	6.0	6.6
Fe (wt%)	49.4	49.6
Observed Li/Fe ratio	0.98	1.06
C (wt%)	1.24	2.37
Sample density	4.13	3.75
Li_2CO_3 (wt%)	7.6 (or less)	14.6 (or less)
Recalculated Li/Fe ratio	0.75 (or more)	0.63 (or more)
Phase composition calculated from wt%	$Li_{0.75}H_{0.25}FeO_2$	$Li_{0.63}H_{0.37}FeO_2$

was obtained, in a dry box, by reacting lithium foil with anhydrous ethanol. The expected topotactic reactions are:

$$170\ °C,\ 15\ h$$
$$\alpha\text{-FeOOH} + C_2H_5OLi \rightarrow r\text{-LiFeO}_2 + C_2H_5OH$$
$$140\ °C,\ 15\ h$$
$$\gamma\text{-FeOOH} + C_2H_5OLi \rightarrow o\text{-LiFeO}_2 + C_2H_5OH$$

After reaction, the suspensions were filtered, washed with ethanol and dried under vacuum (10^{-3} Torr) for 24 h in order to eliminate any trace of solvent. This procedure was initiated after mass spectroscopy–coupled thermal analyses had shown the presence of adsorbed ethanol and CO_2 in the samples. In order to prevent phase transitions as observed by X-ray diffraction, their drying was carried out at 250 and 100 °C for r-$Li_{0.80}H_{0.20}FeO_2$ and o-$Li_{0.70}H_{0.30}FeO_2$, respectively, higher temperatures leading to α-$LiFeO_2$ in both cases.

2.2 Characterization

Phase compositions were determined using the complementary techniques of density measurements, quantitative and thermal analyses and IR spectroscopy. The densities were measured using an automatic gas pycnometer (ACCUPYC 1330). Fe and Li analyses were performed with the use of a plasma

emission spectrometer, and the carbon content of the samples was determined with a carbon microanalysis system (Table 1). The presence of by-products could be detected by running FTIR spectra (205XC Nicolet spectrometer), and performing TGA and mass spectrometry analyses.

X-Ray diffraction diagrams (40 kV × 30 mA) were recorded in a Bragg–Brentano geometry on a Siemens D5000 diffractometer equipped with a nickel filter. Since the materials present a strong fluorescence under Cu-Kα radiation, long recording times of *ca.* 15 h were used to obtain acceptable signal/noise ratios. The electronic microscopy study was made on a JEOL 6400 F system. Structure determinations were carried out by the Rietveld method using the FULLPROF program.[22]

2.3 Electrochemistry

Charges and discharges of the $Li_{1-x}H_xFeO_2$ phases in $Li_{1-x}H_xFeO_2$/Li systems with a liquid electrolyte have been made in coin-cell generators from the Saft company. These cells were mounted in an argon filled dry box (O_2 and $H_2O \approx 1$ ppm). The cathodes were made from 80% of active materials, 7.5 soot, 7.5 graphite and 5% Teflon emulsion according to a procedure described elsewhere.[23] The anode was a disk of lithium metal (diameter = 15 mm). The electrolyte was polypropylene carbonate (PC)–ethylene carbonate (EC)–dimethyl carbonate (DMC) (1:1:3 v/v) in which 1 M $LiPF_6$ was dissolved. The batteries were tested using a MAC PILE apparatus working in the potentiostatic mode (5 mV h^{-1}).

3 Results and discussion

3.1 Synthesis and characterization

Although the samples were handled in a dry box, IR spectroscopy showed systematically the occurrence of some Li_2CO_3, although this phase would not show up on the XRD diagrams. It was assumed that this was due to the amorphous state of the phase. Li_2CO_3 could have formed upon reaction of CO_2 contained in air on the phases during the XRD recording, on some amount of unreacted lithium ethanoate, or on some degradation products (see below).

Assuming that all the carbon found through elemental analysis arose from Li_2CO_3, the poorest lithium concentrations were calculated (Table 1), *i.e.* r-$Li_{0.75}H_{0.25}FeO_2$ and o-$Li_{0.63}H_{0.37}FeO_2$. The remaining protons indicate an incomplete H–Li substitution. Attempts to obtain a more complete reaction by modification of the synthesis conditions (temperature, time, reactants concentrations) failed, and the results presented here correspond to the best substitution rate. The oxidation state of iron was determined by a redox analysis: the exclusive presence of Fe^{3+} was always found, in agreement with the given formulation.

From the densities D_m = 4.13 and 3.75 g cm^{-3} measured for the ramsdellite and orthorhombic phases, respectively, and considering the samples as a mixture of Li_2CO_3 and $Li_{1-x}H_xFeO_2$, one can calculate the density of the ramsdellite and orthorhombic phases. The exact amount of Li_2CO_3 is not known, but from the theoretical density of $LiFeO_2$ calculated from the crystal cell, solving the problem of the phase composition is possible. The following results were obtained: r-$Li_{0.80}H_{0.20}FeO_2$: D_c = 4.35 g cm^{-3} (Li_2CO_3 = 5.0%), o-$Li_{0.70}H_{0.30}FeO_2$: D_c = 4.25 g cm^{-3} (Li_2CO_3 = 11.9%).

The calculated carbonate concentrations are in reasonable agreement with the analyses given in Table 1. Considering that all materials were handled in dry inert gas, it was thought that the occurrence of so much lithium salt had to originate from the degradation of C_2H_5OLi during the synthesis. The heating of lithium ethanoate alone in ethanol in an autoclave for one day at 170 °C yielded a white powder the elemental analysis

of which pointed to the presence of salts other than C_2H_5OLi. The best fit was found to correspond to 87.8% C_2H_5OLi, 4.3% Li_2CO_3 and 7.9% LiOH, with the following elemental analyses: Calc. (found) C, 41.3 (40.2); Li, 14.8 (14.3); O, 35.1 (36.7, by difference); H, 8.8 (8.8%). This may explain the astonishingly large amount of carbonate inferred from the density measurements. From these data and from the carbonate content, it is also possible to calculate the composition of the $Li_{1-x}H_xFeO_2$ materials. For the ramsdellite phase, the compositions $Li_{0.83}H_{0.17}FeO_2$ and $Li_{0.82}H_{0.18}FeO_2$ were obtained. Averaging with the limit composition determined from the analytical data ($Li_{0.75}H_{0.25}FeO_2$) the formula $Li_{0.80}H_{0.20}FeO_2$ can be confidently proposed for the first material. For the second, the calculations yielded $Li_{0.74}H_{0.26}FeO_2$ and $Li_{0.72}H_{0.28}FeO_2$ which, with the first determination ($Li_{0.63}H_{0.37}FeO_2$), leads to $Li_{0.70}H_{0.30}FeO_2$. In the following, the two materials under study will then be referred to as r-$Li_{0.80}H_{0.20}FeO_2$ and o-$Li_{0.70}H_{0.30}FeO_2$.

3.2 Structure refinement

With the SEARCH program (from SOCABIM), some impurities could be detected in the r-$Li_{0.80}H_{0.20}FeO_2$ sample. They were Fe_2O_3 and KCl initially contained in the α-FeOOH precursor (Fig. 1) [α-FeOOH is prepared by reaction of $Fe(OH)_3$ with KOH followed by a washing with an NH_4Cl aqueous solution, then a final washing by H_2O].

Despite with the poor crystallinity of the phases (Fig. 1 and 2), the structure determinations were performed successfully from the XRD powder diagrams of r-$Li_{0.80}H_{0.20}FeO_2$ (original work) and o-$Li_{0.70}H_{0.30}FeO_2$.[2] However, the occupation ratios of the cationic sites filled by Li and H were not refined: they were fixed at the lithium analytical concentration (Occupancy = 0.8 and 0.7, respectively). In addition, the isotropic atomic displacement parameters were set to those values found for the same elements in parent compounds. Tables 2–4 give the recording and refinement conditions and the atomic position parameters (0.8 Å^2 for Fe and 1 Å^2 for the other elements).

The structure of r-$Li_{0.80}H_{0.20}FeO_2$ is indeed isotypic of its precursor α-FeOOH. Only the cell parameters had been previously refined by Sakurai *et al.*[17] The Rietveld refinement allowed, after Brindley corrections, determination of the amount of Fe_2O_3 and KCl impurities which were 6.2 and 0.6% respectively. A new calculation of the density on r-$Li_{0.80}H_{0.20}FeO_2$ considering these phases did not change meaningfully the previously calculated phase composition.

In a first approach, the structure of r-$Li_{0.80}H_{0.20}FeO_2$ is similar to that of α-FeOOH (Fig. 3) with an association of
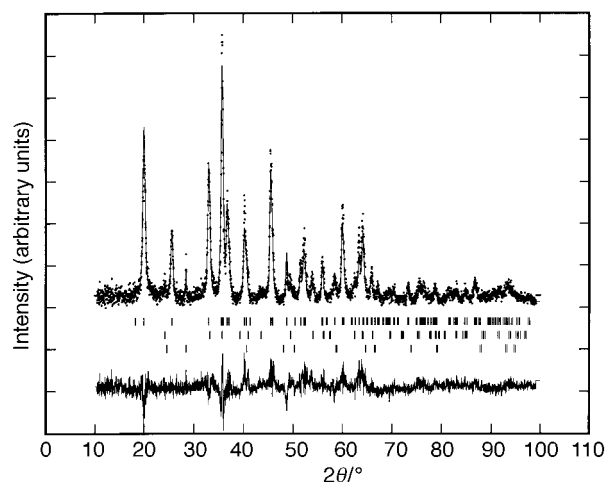

Fig. 1 X-Ray diffraction diagram of r-$Li_{0.80}H_{0.20}FeO_2$. Tick marks: first = r-$Li_{0.80}H_{0.20}FeO_2$, second = Fe_2O_3, third = KCl.
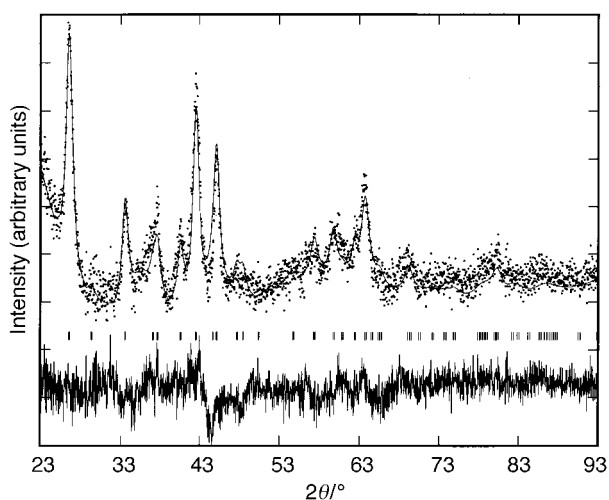
Fig. 2 X-Ray diffraction diagram of o-Li$_{0.70}$H$_{0.30}$FeO$_2$.

Table 2 Rietveld recording conditions and refinement results for r-Li$_{0.80}$H$_{0.20}$FeO$_2$. Owing to the small amount of both Fe$_2$O$_3$ and KCl in the sample, their Caglioti function was chosen to be constant with 2θ (w is the only refined parameter)

Data collection
Wavelengths: 1.54060, 1.54439 Å
Angular range: 2θ min: 10°, 2θ max: 99.97°
Step, time per step: 0.03° (2θ), 12 s

Results of refinement
Space group: r-Li$_{0.80}$H$_{0.20}$FeO$_2$: *Pnma*, Fe$_2$O$_3$: *R$\bar{3}$c*, KCl: F*m$\bar{3}$m*
Number of refined parameters: 28
r-Li$_{0.80}$H$_{0.20}$FeO$_2$: 17, Fe$_2$O$_3$: 7, KCl: 3
Number of reflections:
r-Li$_{0.80}$H$_{0.20}$FeO$_2$: 172, Fe$_2$O$_3$: 72, KCl: 30
Results of wt% after Brindley corrections:
r-Li$_{0.80}$H$_{0.20}$FeO$_2$: 93.2, Fe$_2$O$_3$: 6.2, KCl: 0.6

Profile parameters for r-Li$_{0.80}$H$_{0.20}$FeO$_2$
Cell parameters: $a=9.718(2)$, $b=2.9354(5)$, $c=5.0095(9)$ Å
Volume, Z: 142.89(6) Å^3, 4
η(Pseudo-Voigt): 0.56(3)
Halfwidth parameters (U,V,W): 1.6(2), −1.6(2), 0.57(3)
Preferred orientation: 0.913(8) along (0,1,0)

Profile parameters for Fe$_2$O$_3$
Cell parameters: $a=5.035(2)$, $c=13.771(8)$ Å
Volume, Z: 302.408 Å^3, 6
η(Pseudo-Voigt): 0.5
Halfwidth parameters (U,V,W): 0, 0, 0.21(2)

Profile parameters for KCl
Cell parameter: $a=6.286(2)$ Å
Volume, Z: 248.424 Å^3, 4
η(Pseudo-Voigt): 0.5
Halfwidth parameters (U,V,W): 0, 0, 0.028(9)

Global parameters
Cosθ shift parameters: 0.028(6)

Reliability factors
with structure constraint: $R_p=0.108$, $R_{wp}=0.136$, $\chi^2=1.24$
r-Li$_{0.80}$H$_{0.20}$FeO$_2$: $R_B=0.174$, $R_F=0.142$
Fe$_2$O$_3$: $R_B=0.208$, $R_F=0.187$
KCl: $R_B=0.183$, $R_F=0.186$

Table 3 Rietveld recording conditions and refinement results for o-Li$_{0.70}$H$_{0.30}$FeO$_2$

Data collection
Wavelengths: 1.54060, 1.54439 Å
Angular range: 2θ min: 10°, 2θ max: 99.97°
Step, time per step: 0.03° (2θ), 12 s

Results of refinement
Space group: o-Li$_{0.70}$H$_{0.30}$FeO$_2$: *Pmmn*
Number of refined parameters:
o-Li$_{0.70}$H$_{0.30}$FeO$_2$: 14
Number of reflections:
o-Li$_{0.70}$H$_{0.30}$FeO$_2$: 105

Profile parameters for o-Li$_{0.70}$H$_{0.30}$FeO$_2$
Cell parameters: $a=4.019(1)$, $b=2.973(1)$, $c=6.091(4)$ Å
Volume, Z: 72.81(6), 2
η(Pseudo-Voigt): 0.89(4)
Halfwidth parameters (U,V,W): 5(1), −4.0(9), 1.5(1)
Preferred orientation: 1.18(1) along (0,0,1)

Global parameters
Cosθ shift parameters: −0.11(1)

Reliability factors
With structure constraint: $R_p=0.013$, $R_{wp}=0.017$, $\chi^2=2.54$
o-Li$_{0.70}$H$_{0.30}$FeO$_2$: $R_B=0.26$, $R_F=0.21$

Table 4 Atomic position parameters of r-Li$_{0.80}$H$_{0.20}$FeO$_2$ and o-Li$_{0.70}$H$_{0.30}$FeO$_2$

r-Li$_{0.80}$H$_{0.20}$FeO$_2$

Atom	x	y	z	B/Å^2	Occupancy
Fe	0.1335(4)	1/4	0.0772(9)	0.8	1
O1	0.005(1)	3/4	0.262(2)	1	1
O2	0.256(1)	1/4	0.405(5)	1	1
Li	0.396(5)	1/4	0.08(1)	1	0.8

oLi$_{0.70}$H$_{0.30}$FeO$_2$

Atom	x	y	z	B/Å^2	Occupancy
Fe	1/4	1/4	0.657(1)	0.8	1
O1	3/4	1/4	0.151(4)	1	1
O2	3/4	1/4	0.619(4)	1	1
Li	1/4	1/4	0.13(1)	1	0.7

(2.08 Å for both). The more important Li–O distance dispersion may be attributed to the poor accuracy on the lithium position. The differences between theoretical and observed diagrams are likely due to stacking faults and/or crystallite size anisotropy that change greatly the diffraction diagram line profiles.

The o-Li$_{0.70}$H$_{0.30}$FeO$_2$ structure is also isotypical of that of γ-FeOOH (Fig. 4). The structural determination has allowed us to confirm the orthorhombic structure found by Kanno *et al.*[18] (Tables 3 and 4). This structure is made of corrugated planes of [FeO$_6$] octahedra with the lithium anions occupying the interplane octahedral sites. The mean <Fe–O> and <Li–O> distances are 2.05 and 2.13 Å. No impurity other than Li$_2$CO$_3$ was found in the samples.

3.3 Morphological features

Scanning electron microscopy studies have been carried out to characterize the powders (Fig. 5). The α-FeOOH precursor and r-Li$_{0.80}$H$_{0.20}$FeO$_2$ phase show clear morphological similarities: both phases are very homogeneous with very small crystal sizes (lengths of *ca.* 0.4 and widths of *ca.* 0.05 μm). The same resemblance exists between γ-FeOOH and o-Li$_{0.70}$H$_{0.30}$FeO$_2$ with lengths and widths of *ca.* 0.1 and *ca.* 0.03 μm, respectively, *i.e.* smaller than for the first two compounds. These observations point to the topotactical nature of the proton substitution for lithium whereas the small size of the crystals should insure a good electrochemical reactiv-
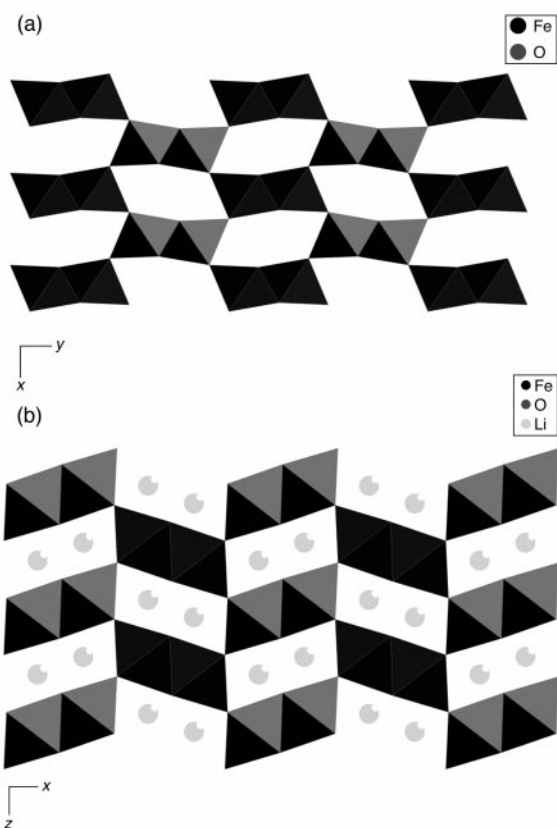
[FeO$_6$] octahedra forming (1 × 2) tunnels in which lithium lies in octahedral sites. However, if the XRD powder diagrams of r-Li$_{0.80}$H$_{0.20}$FeO$_2$ and α-FeOOH are compared, there appear to be important hierarchy differences that are reminiscent of stacking faults of the pyrolusite type or of microtwinning. In fact, this difference stems from the important tilt of the double octahedra groups, the (1 × 2) tunnels becoming misaligned in the iron derivative and forming chevrons.

The [FeO$_6$] and [LiO$_6$] octahedra are slightly distorted with mean <Fe–O> and <Li–O> distances in the expected range

Fig. 3 Structures of (a) the precursor α-FeOOH and (b) r-$Li_{0.80}H_{0.20}FeO_2$.

ity of the $Li_{1-x}H_xFeO_2$ phases respective to the lithium intercalation/deintercalation process because of the small diffusion path.

Electrochemistry: results and discussion

The conductivities of r-$Li_{0.80}H_{0.20}FeO_2$ and o-$Li_{0.70}H_{0.30}FeO_2$, which have been determined by a simple measure on stacked powders are *ca.* 10^{-10} S cm^{-1}. This very small value, which is in agreement with the red–brown color of the materials, is much smaller than that of black–green o-$LiMnO_2$ (10^{-6} S cm^{-1}): it may explain, in part, the strong polarization during the first charge (see below).

The charge curve of the two $Li_{1-x}H_xFeO_2$ phases is similar with a high mean potential (4.1 V) that could correspond to the oxidation of Fe^{3+} to Fe^{4+} (Fig. 6). Electrochemical tests performed on both materials showed them to be very similar, and only the various analytical techniques (XRD, iron analyses, Mössbauer spectroscopy) carried out on r-$Li_{0.80}H_{0.20}FeO_2$ which has not been subject of much study,[17] are reported below. Analyses of Fe and Li indicate a lithium deintercalation (Fig. 7) which is confirmed by the amorphisation of the material with the occurrence of a wide hump below the unaltered peaks of the starting material.

The discharge curves exhibit a mean potential reminiscent of the Fe^{3+}/Fe^{2+} couple. Clearly, the first oxidation is not reversible (and not complete) and it appears that the deintercalated phase is not stable. Obviously, the discharge does not take place on the charged material itself but on one of its degraded forms (assuming that the formed Fe^{4+} ions oxidize the electrolyte to produce Fe^{3+} species) and/or on the remaining $Li_{1-x}H_xFeO_2$ that is evidenced on the XRD diagrams. Indeed, a discharge of the starting material itself gives a curve that is very close to that of the first discharge of the $Li_{1-x}H_xFeO_2$ materials (Fig. 8). These similarities point to

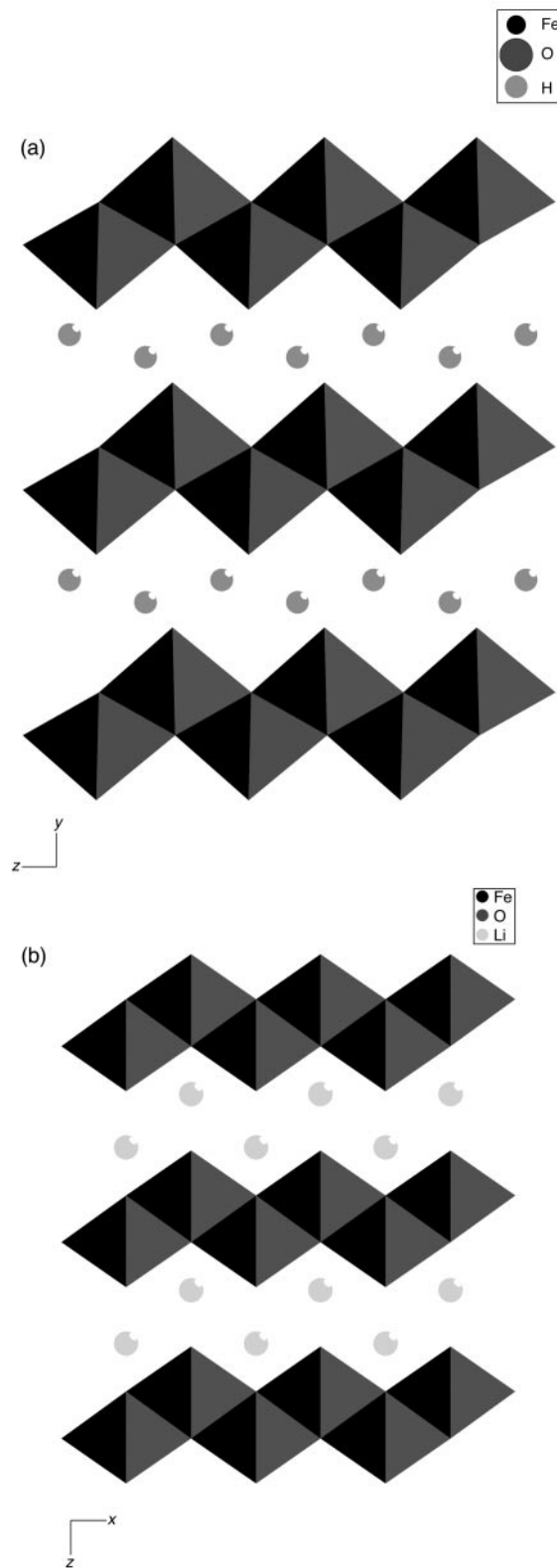**Fig. 4** Structures of (a) the precursor γ-FeOOH and (b) o-$Li_{0.70}H_{0.30}FeO_2$.

the reduction of Fe^{3+} species in the discharge of the $Li_{1-x}H_xFeO_2/Li$ batteries. For o-$Li_{0.70}H_{0.30}FeO_2$, the first charge curve [Fig. 6(b)] corresponds to a capacity (1 F) higher than the phase lithium content, thus confirming the oxidation of the electrolyte. In order to check that the instability of Fe^{4+} formed from the $Li_{1-x}H_xFeO_2$ phases was not due to the nature of the electrolyte, the same study was carried out using $LiPF_6$ dissolved in acetonitrile, with V_2O_5 as anode (to avoid
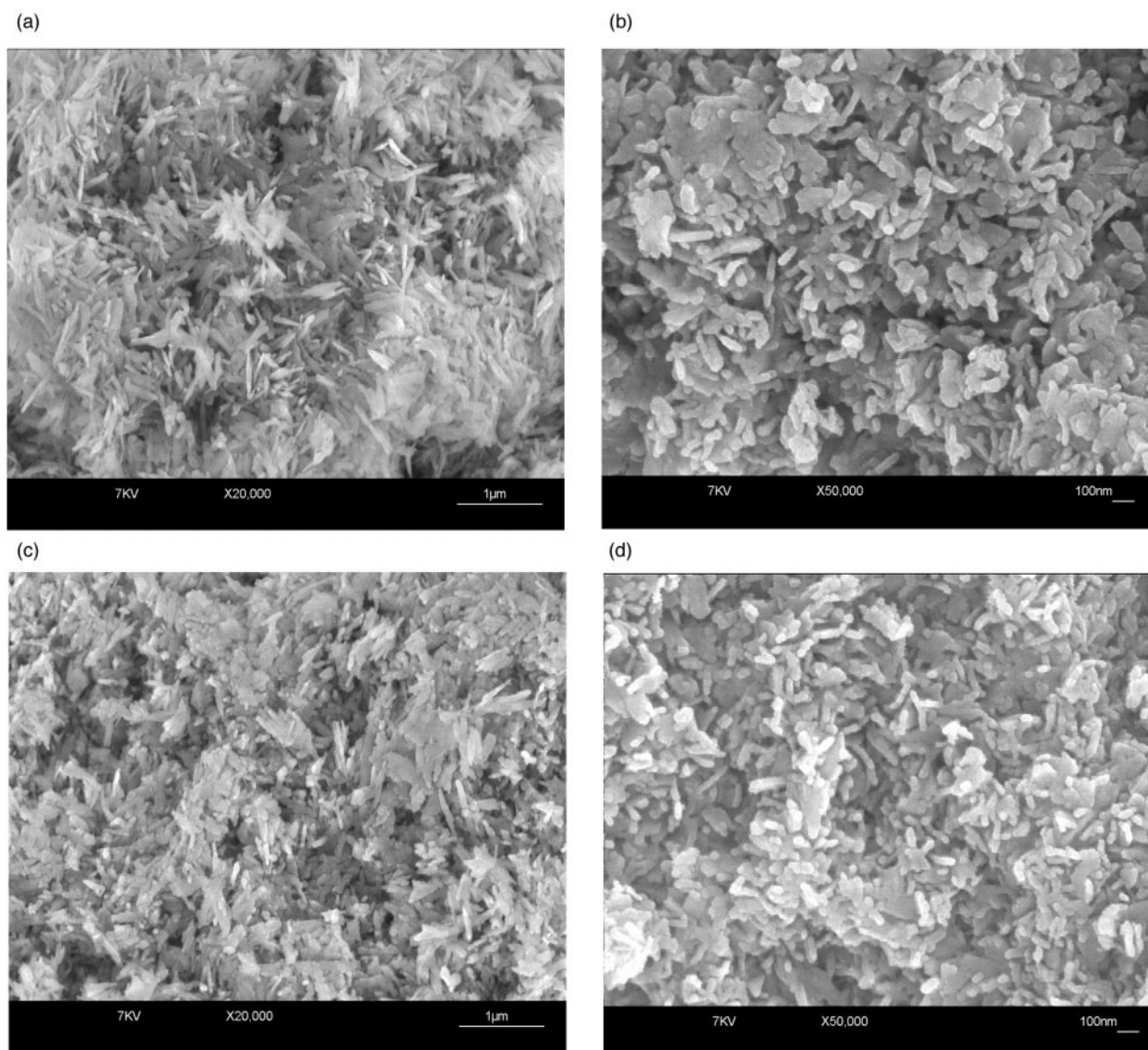
Fig. 5 Scanning microscopy photographs of (a) the precursor α-FeOOH, (b) γ-FeOOH, (c) r-Li$_{0.80}$H$_{0.20}$FeO$_2$ and (d) o-Li$_{0.70}$H$_{0.30}$FeO$_2$.

electrolyte polymerisation in the presence of lithium). This study delivered the same type of results with a low mean potential discharge (*ca.* 2.5 V *vs.* Li$^+$/Li) (Fig. 9). The shape of all these curves is in agreement with those published by Kanno *et al.*[16–18] and Sakurai[17] who had used LiClO$_4$ dissolved in a mixture of propylene carbonate and dimethyl ethylene. Clearly, Fe^{4+} does appear unstable in this electrolyte as well and in the potential range used. In addition to the electrolyte oxidation, the strong polarization observed in the first charges may also originate from the slower diffusion of lithium, in relation with the presence of residual protons in the Li$_{1-x}$H$_x$FeO$_2$ phases and with the strong resistivity of the material. The instability of Fe^{4+} thus prevents the functioning of the systems on the Fe^{4+}/Fe^{3+} couple.

3.5 Mössbauer spectroscopy

A Mössbauer study was performed on charged r-Li$_{0.80}$H$_{0.20}$FeO$_2$ in order to detect the possible presence of Fe^{4+}. Among three samples (Fig. 10), two were charged in the LiPF$_6$–PC–EC–DMC electrolyte, one up to 4.2 V (r1) the other up to 5 V (r2), whereas the third was oxidized in a LiPF$_6$–acetonitrile electrolyte with V$_2$O$_5$ as anode up to 1.7 V (r3). In a first step, the Mössbauer spectrum of sample r2 was recorded at 293 K at high velocity (12 mm s^{-1}) (Fig. 11). The spectrum shows two components, the major one being constituted of a quadrupolar doublet (D), and the minor one corresponding to a sextuplet (S). Component D is attributable to Fe^{3+} in a paramagnetic state whereas component S corresponds to Fe^{3+} in a room temperature magnetically ordered state. It is possible to detect in this sample the occurrence, at a very small level (a few %), of iron belonging unambiguously to the spinel phase LiFe$_5$O$_8$. This phase is probably present in the product as an amorphous phase since it was not detected by XRD. The main interest of this wide range spectrum was to evidence this impurity in the compound to take into account the corresponding lines in the spectrum. Such wide range spectra have also been collected for r1 and r3 samples but they are not presented here due to the very small amount of impurity found in these samples.

The three Mössbauer spectra of r1, r2 and r3 were then recorded at 293 K at low velocity (2 mm s^{-1}) (Fig. 12). These spectra are composed of two wide, asymmetric lines. On each side of these lines appear two shoulders (hardly detectable on some spectra) that correspond to the internal lines of the sextuplet (S) observed in the spectra recorded at high speed for r2. These spectra have been fitted with a model implying a quadrupole splitting. Because of the important width of the absorption doublet, all of the three spectra fittings required
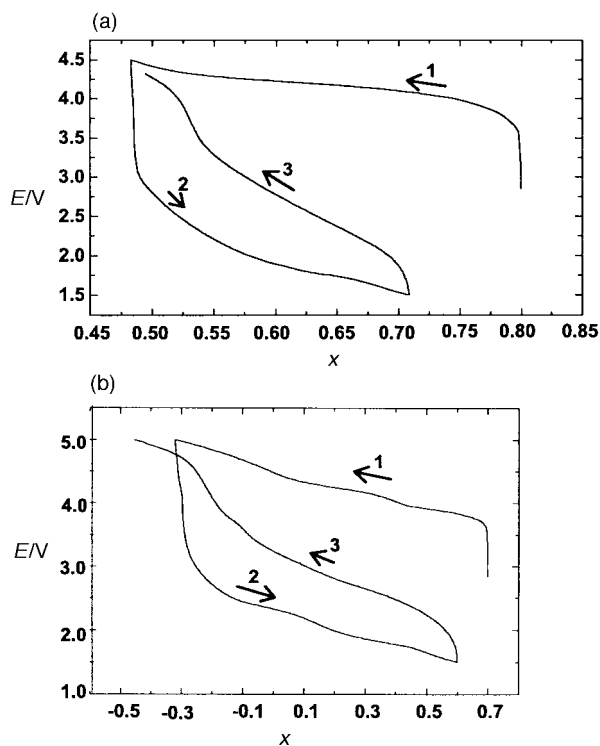
Fig. 6 Charge (1,3) and discharge (2) curves of (a) r-$Li_{0.80}H_{0.20}FeO_2$ and (b) o-$Li_{0.70}H_{0.30}FeO_2$.
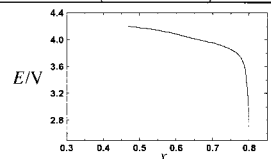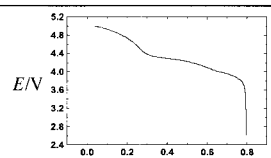
Fig. 7 Analytical and XRD data recorded for charged r-$Li_{0.80}H_{0.20}FeO_2$ oxidized at 4.2 V and 5 V potential limits.

Fig. 8 Discharge (1) and charge (2) curves of (a) r-$Li_{0.80}H_{0.20}FeO_2$ and (b) o-$Li_{0.70}H_{0.30}FeO_2$.

Fig. 9 Charge (1,3) and discharge (2) curves of r-$Li_{0.80}H_{0.20}FeO_2$ with $LiPF_6$ dissolved in acetonitrile as electrolyte and V_2O_5 as anode (potential *vs.* Li^+/Li).

the use of two quadrupole splitting distributions (isomeric shift δ_1 and δ_2). In addition, for samples r2 and r3, the two internal lines of the sextuplet (S) had to be taken into account. These contributions belonging to $LiFe_5O_8$ are not presented in Table 5 because this compound is not electrochemically active. For r1, the very important widening of the paramagnetic peaks somewhat obscure these two lines. With an isomer shift of $\delta_1 = 0.38$ mm s^{-1}, distribution 1 (Table 5) corresponds to high spin Fe^{3+} in a distorted octahedral environment. Distribution 2 has an isomeric shift of $\delta_2 = 0.1$ mm s^{-1} which does not match that of Fe^{3+} in an octahedral coordination sphere (at 293 K, the isomer shift for an oxygen matrix should lie between 0.3 and 0.4 mm s^{-1}). It can only correspond either to Fe^{3+} in a tetrahedral coordination environment or to a mean oxidation state of iron of $+3.5$, the sampling time of Mössbauer being greater than the electronic relaxation time between Fe^{3+} and Fe^{4+}. The first hypothesis could be explained by the presence of some $LiFe_5O_8$ that contains Fe^{3+}
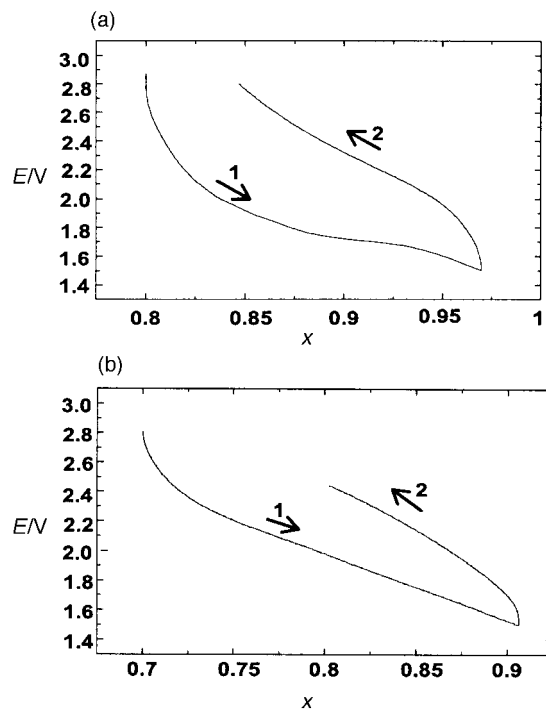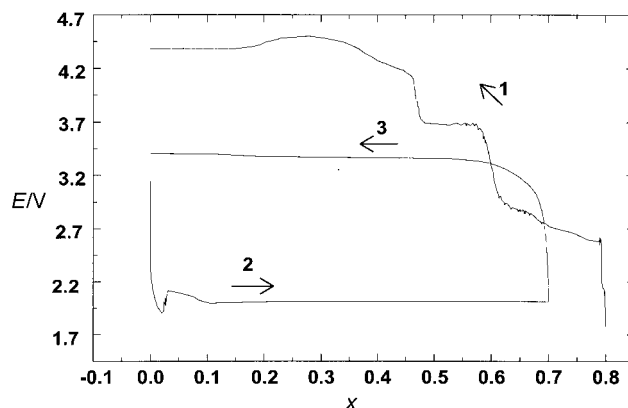
ions in tetrahedra. However, due to the small concentration of this impurity only the second hypothesis can be realistically considered and is in agreement with a number of Mössbauer studies made on iron containing cathodic materials which have shown that Fe^{4+} is observed in a localized state at 293 K only for very oxidized phases.[24] The amount of Fe^{4+} could be determined from distribution 2 of the Mössbauer spectra recorded at 293 K (Table 5) for all the samples r1, r2 and r3.

A Mössbauer spectrum has been recorded at 4.2 K on r2 in order to confirm the hypothesis of a mean oxidation state $Fe^{3.5+}$, through a localization of Fe^{4+} at low temperature. The recorded spectrum (Fig. 13) shows three components, two magnetic ones (two sextuplets) and a paramagnetic one with a very weak intensity yet quite visible in the middle of the spectrum. Corresponding Mössbauer characteristics are listed in Table 6. This spectrum was fitted with two hyperfine field distributions, one related to Fe^{3+} (89% intensity) and the other to localized low temperature Fe^{4+} (8% intensity). The paramagnetic part (3%), due to fine grains, characterizes a superparamagnetic behavior. The amount of Fe^{4+} observed at 4.2 K is close enough to half that of $Fe^{3.5+}$ (18%) determined
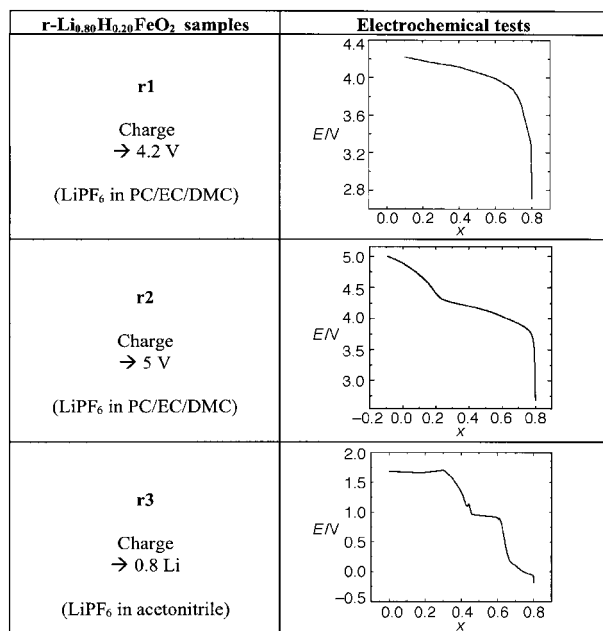
r-$Li_{0.80}H_{0.20}FeO_2$ samples	Electrochemical tests
r1 Charge → 4.2 V ($LiPF_6$ in PC/EC/DMC)	
r2 Charge → 5 V ($LiPF_6$ in PC/EC/DMC)	
r3 Charge → 0.8 Li ($LiPF_6$ in acetonitrile)	

Fig. 10 Charge curves of the r1, r2 and r3 cathodes used for the Mössbauer spectroscopy study.

Fig. 11 Room temperature Mössbauer spectrum recorded at high velocity (± 12 mm s^{-1}) on oxidized r2.

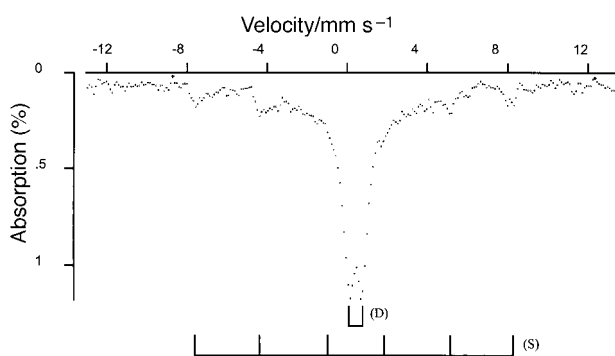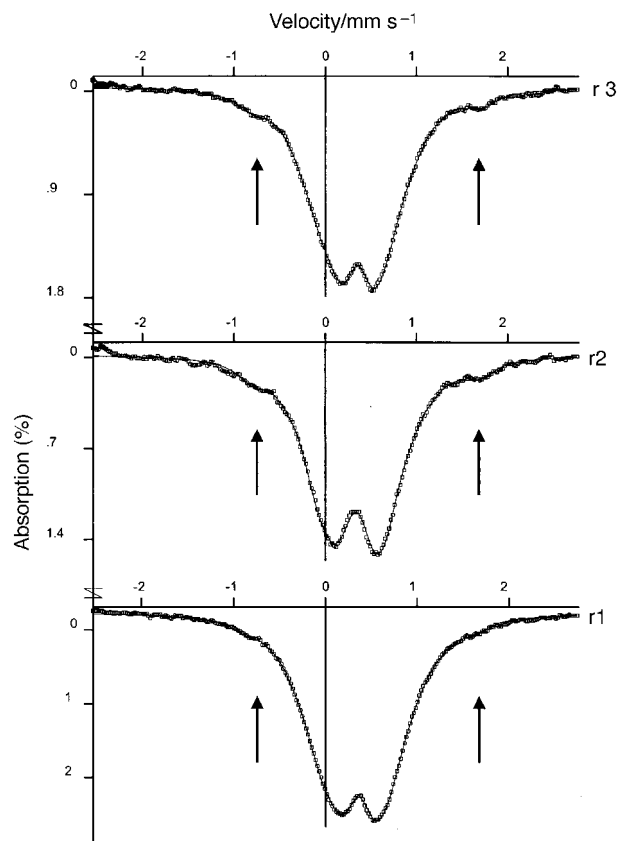**Fig. 12** Room temperature Mössbauer spectra recorded at low velocity (± 200 mm s^{-1}) on oxidized r1, r2 and r3.

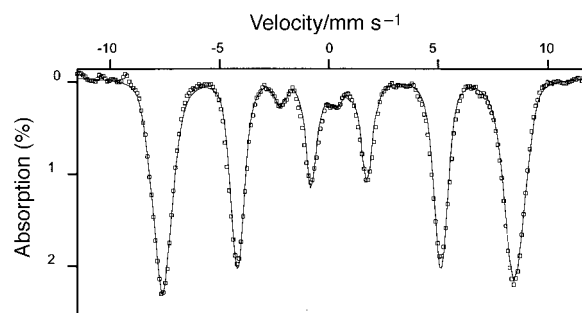**Fig. 13** 4.2 K Mössbauer spectrum recorded at high velocity (± 12 mm s^{-1}) on oxidized r2.

at 293 K, thus confirming this assignment in the oxidized cathodes r1, r2 and r3.

The amount of Fe^{4+} deduced from the three Mössbauer spectra at room temperature (Table 5), is much less than the charge in F measured from the electrochemical oxidation curves. However, the amount of Fe^{4+} evaluated by Mössbauer spectroscopy does increase with the charge passed. All these observations confirm the removal of lithium from r-$Li_{0.80}H_{0.20}FeO_2$ during the first charge and the reduction of a large fraction of Fe^{4+} formed into Fe^{3+}. As assumed above,

this implies that the following discharges must correspond to the reduction of Fe^{3+} into Fe^{2+}. The nature of the electrolyte does not alter the parasitic reduction at the first charge since the amount of Fe^{4+} is about the same for the sample tested with acetonitrile. The amorphisation observed on cycling (see

Table 5 Room temperature Mössbauer data and interpretation made on oxidized samples r1, r2 and r3

Sample r-$Li_{0.80}H_{0.20}FeO_2$	Distribution 1			Distribution 2		
	δ_1/mm s^{-1}	$<\Delta_1>$/mm s^{-1}	A_1 (%)	δ_2/mm s^{-1}	$<\Delta_2>$/mm s^{-1}	A_2 (%)
r1	0.38	0.65	87	0.1	0.58	13
r2	0.38	0.70	82	0.1	0.66	18
r3	0.38	0.73	88	0.1	0.60	12

Sample	Number of F deduced from electrochemical tests	Amount of Fe^{4+} (%) determined from Mössbauer spectra
r1	0.7	6.5
r2	0.9	9
r3	0.8	6

Table 6 4.2 K Mössbauer spectra interpretation made on oxidized sample r2

Sextuplet 1				Sextuplet 2				Doublet			
δ_1/mm s^{-1}	B_1/T	Γ_1/mm s^{-1}	A_1 (%)	δ_2/mm s^{-1}	B_2/T	Γ_2/mm s^{-1}	A_2 (%)	δ_3/mm s^{-1}	Δ_3/mm s^{-1}	Γ_3/mm s^{-1}	A_3 (%)
0.49	50.2	0.30	89	0.03	27.8	0.30	8	0.44	0.67	0.30	3

above) reflects the destruction of the pristine material, although some authors consider it as the result of a phase transition.[25,26]

Conclusion

The characterization of the two varieties r-$Li_{0.80}H_{0.20}FeO_2$ and o-$Li_{0.70}H_{0.30}FeO_2$ have been carried out more completely than in previous studies. The chemical compositions have been determined in a more accurate fashion, the structure of r-$Li_{0.80}H_{0.20}FeO_2$ has been refined for the first time and that of o-$Li_{0.70}H_{0.30}FeO_2$ has been confirmed. The two phases have been compared in their structure and powder morphology, showing for both materials very small crystal sizes similar to those of the precursors. The poor cycling of the two materials is explained by the instability of the Fe^{4+} species in the media and potential ranges used, as found from the analytical, electrochemical and spectroscopic studies. The same kind of work done on α-$LiFeO_2$[27] completely confirms the intrinsic instability of Fe^{4+} in $LiFeO_2$–organic electrolyte–Li systems.

References

1 D. E. Cox, G. Shirane, P. A. Flinn, S. L. Rubu and W. J. Takei, *Phys. Rev.*, 1963, **134**, 1547.
2 J. C. Anderson and M. Schieber, *J. Phys. Chem. Solids*, 1964, **25**, 961.
3 J. C. Anderson, S. K. Dey and V. Halpern, *J. Phys. Chem. Solids*, 1965, **26**, 1555.
4 R. Famery, P. Bassoul and F. Queyroux, *J. Solid State Chem.*, 1984, **57**, 178.
5 S. Kikkawa, H. Ohkura and M. Koizumi, *Mater. Chem. Phys.*, 1987, **18**, 375.
6 C. Barriga, V. Barron, R. Gancedo, M. Gracia, J. Morales, J. L. Tirado and J. Torrent, *J. Solid State Chem.*, 1988, **77**, 132.
7 C. Barriga, J. Morales and J. L. Tirado, *Mater. Res. Bull.*, 1990, **25**, 997.
8 M. Tabuchi, K. Ado, H. Sakaebe, C. Masquelier, H. Kageyama and O. Nakamura, *Solid State Ionics*, 1995, **79**, 220.
9 S. Uchida, H. Kashiwagi, T. Sato and A. Okuwaki, *J. Mater. Sci.*, 1996, **31**, 3827.
10 V. B. Nalbandyan and I. L. Shukaev, *Russ. J. Inorg. Chem.*, 1987, **32**, 453.
11 N. Imanishi, K. Nakhara, Y. Takeda, O. Yamamoto and M. Takano, *Denki Kagaku*, 1993, **61**, 1451.
12 Y. Takeda, K. Nakahara, M. Nishijima, N. Imanishi, O. Yamamoto, M. Takano and R. Kanno, *Mater. Res. Bull.*, 1994, **29**, 659.
13 B. Fuchs and S. Kemmler-Sack, *Solid State Ionics*, 1994, **68**, 279.
14 T. Shirane, R. Kanno, Y. Kawamoto, Y. Takeda, M. Takano, T. Kamiyama and F. Izumi, *Solid State Ionics*, 1995, **79**, 227.
15 R. Kanno, *Denki Kagaku*, 1995, **63**, 778.
16 R. Kanno, T. Shirane and Y. Kawamoto, *J. Power Sources*, 1997, **68**, 145.
17 Y. Sakurai, H. Arai, S. Okada and J. Yamaki, *J. Power Sources*, 1997, **68**, 711.
18 R. Kanno, T. Shirane, Y. Kawamoto, Y. Takeda, M. Takano, M. Ohashi and Y. Yamaguchi, *J. Electrochem. Soc.*, 1996, **143**, 2435.
19 M. Tabuchi, C. Masquelier, T. Takeuchi, K. Ado, I. Matsubara, T. Shirane, R. Kanno, S. Tsutsui, S. Nasu, H. Sakjaebe and O. Nakamura, *Solid State Ionics*, 1996, **90**, 129.
20 K. Ado, M. Tabuchi, H. Kobayashi, H. Kageyama and O. Nakamura, *J. Electrochem. Soc.*, 1997, **144**, L177.
21 G. Brauer, *Handbook of Preparative Inorganic Chemistry*, Academic Press, New York, 1965, vol. 2, p. 1491.
22 J. Rodriguez Carjaval, *Physica B*, 1993, **192**, 55.
23 L. Croguennec, P. Deniard, R. Brec, P. Biensan and M. Broussely, *Solid State Ionics*, 1996, **89**, 127.
24 L. Guerlou-Demourgues, L. Fournès and C. Delmas, *J. Electrochem. Soc.*, 1996, **143**, 3083.
25 R. Kanno, T. Shirane, Y. Inaba and Y. Kawamoto, *J. Power Sources*, 1997, **68**, 145.
26 Y. Sakurai, H. Arai, S. Okada and J. Yamaki, *J. Power Sources*, 1997, **68**, 711.
27 L. Bordet-Le Guenne, unpublished results.